

Magnetic Hysteresis Modeling with Neural Operators

Abhishek Chandra^{1,2}, *Graduate Student Member, IEEE*, Bram Daniels¹, *Graduate Student Member, IEEE*, Mitrofan Curti^{1,2}, *Member, IEEE*, Koen Tiels^{2,3}, *Member, IEEE*, and Elena A. Lomonova^{1,2}, *Senior Member, IEEE*

¹Department of Electrical Engineering, Eindhoven University of Technology, 5612 AP Eindhoven, The Netherlands

²Eindhoven Artificial Intelligence Systems Institute, Eindhoven University of Technology, 5612 AP Eindhoven, The Netherlands

³Department of Mechanical Engineering, Eindhoven University of Technology, 5600 MB Eindhoven, The Netherlands

Hysteresis modeling is crucial to comprehend the behavior of magnetic devices, facilitating optimal designs. Hitherto, deep learning-based methods employed to model hysteresis, face challenges in generalizing to novel input magnetic fields. This paper addresses the generalization challenge by proposing neural operators for modeling constitutive laws that exhibit magnetic hysteresis by learning a mapping between magnetic fields. In particular, two prominent neural operators—deep operator network and Fourier neural operator—are employed to predict novel first-order reversal curves and minor loops, where novel means they are not used to train the model. In addition, a rate-independent Fourier neural operator is proposed to predict material responses at sampling rates different from those used during training to incorporate the rate-independent characteristics of magnetic hysteresis. The presented numerical experiments demonstrate that neural operators efficiently model magnetic hysteresis, outperforming the traditional neural recurrent methods on various metrics and generalizing to novel magnetic fields. The findings emphasize the advantages of using neural operators for modeling hysteresis under varying magnetic conditions, underscoring their importance in characterizing magnetic material based devices.

Index Terms—Hysteresis, magnetic materials, neural operators, deep operator network (DeepONet), Fourier neural operator (FNO), rate-independent, generalization.

I. INTRODUCTION

CONTEMPORARY industrialization thrives on magnetic material based devices. Those devices, such as electric machines and actuators, consume more than half of the global electrical energy. Optimizing the performance of these devices includes the estimation of energy dissipated in iron as losses, which is paramount for overall performance. A considerable component of iron loss calculation is the hysteresis loss, approximated through an accurate hysteresis model [1], [2]. A material-specific hysteresis model precisely governs the constitutive relationship between the applied magnetic field (H) and the magnetic flux density (B). The relationship between these fields is nonlinear and history-dependent, traditionally modeled by the Jiles-Atherton [3] and Preisach method [4], among others [5]. Owing to the low inference cost and performance of machine learning based methods in science and engineering, deep learning based methods are frequently applied to model magnetic hysteresis, including but not limited to [6]–[8].

Among the deep learning based methods, recurrent neural architectures present a viable approach for modeling hysteresis due to their inherent reliance on historical data [9]–[13], aligning with the history-dependent nature of hysteresis. However, these architectures primarily achieve accuracy for specific excitations, where predictions are limited to loops for which training has been performed. In real-world scenarios, however, where machine predictions are required for novel acting magnetic fields, generalization—which refers to the ability of deep learning models to predict outside of the training domain [14]—remains an open problem. Consequently, the limitation of current state-of-the-art neural architectures

hinders the generalization across diverse excitation conditions and the estimation of responses for novel H fields, making them unreliable as a part of the magnetic device model.

The limitations of conventional neural networks, including recurrent neural networks (RNN) [15] and their gated variants, such as long short-term memory (LSTM) [16] and gated recurrent unit (GRU) [17], arise from their ability to learn only fixed-dimensional mappings between magnetic fields. These networks cannot model mappings between functions in continuous domains [18], [19]. This paper introduces neural operators [19]–[21] to model the hysteresis relationship between magnetic fields to address these challenges. Unlike conventional neural networks that learn fixed-dimensional mappings, neural operators approximate the underlying operator, representing the mapping between H and B fields, to predict material responses (B fields) for novel H fields. Specifically, neural operators can approximate continuum mappings even when trained on discrete data, allowing them to generalize to novel H fields.

This paper proposes to employ two prominent neural operators—deep operator network (DeepONet) [22] and Fourier neural operator (FNO) [23]—to model the B – H hysteresis relationship. These operator networks are trained to predict novel first-order reversal curves (FORCs) and minor loops not included in the training data. The vanilla versions of DeepONet and FNO are rate-dependent and consider the sampling rate during experiments. Further, to incorporate the rate-independent characteristic prevalent in magnetic hysteresis, this paper introduces a rate-independent Fourier neural operator (RIFNO) to predict B fields when the sampling rates for the H field differ between the training and test data. The primary contributions of this work are outlined as follows:

- This paper proposes an approach shift from learning

a functional approximation between observed magnetic data to learning an operator between magnetic fields to achieve generalization, an important feature that neural magnetic hysteresis models must have.

- The efficiency of neural operators is empirically demonstrated in the context of magnetic hysteresis modeling by comparing it with traditional recurrent neural architectures, highlighting their limitations. Specifically, the results are benchmarked against RNN, LSTM, and GRU models.
- This paper proposes a rate-independent Fourier neural operator to incorporate rate-independent features of magnetic hysteresis and validate its performance through numerical experiments.
- This paper bridges the gap between magnetic hysteresis modeling and scientific machine learning (SciML). We envision that the successful application of neural operators presented in this work will lead to employing and developing advanced neural operator techniques for magnetic hysteresis modeling.

The rest of the manuscript is organized as follows. Section II presents the motivation to employ neural operators for modeling magnetic hysteresis. Section III details the neural operator methodologies employed in this work. Section IV presents a series of numerical experiments conducted to demonstrate the accuracy of neural operators in modeling hysteresis. Section V provides a discussion on the performance and prospects of the proposed approach. The main conclusions drawn from this study are collated in Section VI.

II. MOTIVATION

This section presents the motivation to advocate employing neural operators as surrogates for modeling the hysteresis phenomenon. Hitherto, neural network based function approximation strategies have been utilized to model hysteresis. More generally, traditional neural networks, such as feedforward or recurrent neural networks, leverage the universal function approximation property [24], [25], ensuring that a continuous function f can be learned to approximate the given data pairs (\mathbf{x}_i, y_i) such that $y_i \approx f(\mathbf{x}_i)$ for all N data points, $1 \leq i \leq N$, $i \in \mathbb{Z}$. Here, \mathbf{x}_i and y_i typically represent scalars, vectors, or tensors. The function $f(\mathbf{x}_i)$ is learned as a surrogate for the underlying relationship via a neural network $\mathcal{N}(\mathbf{x}_i, \theta)$, where θ represents the network parameters optimized through a gradient-based optimization method to fit the data. The learned function $f(\mathbf{x}_i)$ effectively maps the finite-dimensional data \mathbf{x}_i to y_i , provided the optimizer finds a suitable local minima by minimizing an appropriate loss function.

In the context of scalar magnetic hysteresis, the data pairs (\mathbf{x}_i, y_i) correspond to (H_i, B_i) , representing the applied magnetic field and induced magnetic field, respectively. These data pairs are often obtained through measurements or numerical models, such as the Preisach model, which acts as a surrogate for lab experiments [6]. The index i denotes the i^{th} measurement datum. The function f encapsulates the hysteresis relationship learned from the provided data pairs. This model is expected to effectively map the finite-dimensional inputs

to finite-dimensional outputs when accurately fitted. However, for novel input fields represented by a distinct H_i sequence, the learned function f fails to approximate the underlying dynamics accurately, as is presented in this work, highlighting a limitation in current strategies.

Why does the function f , approximated through a neural network, fails to predict B fields for novel H excitations? The reason lies in the limited expressive power of traditional neural networks, which are designed to map tensors from the input space (H) to tensors in the output space (B) to learn functions but face challenges in generalizing this concept to map functions to functions [22]. The appropriate mathematical object that satisfies this objective is an operator. An operator $\mathcal{D} : \mathcal{G} \rightarrow \mathcal{H}$ maps a function $g \in \mathcal{G}$ to a function $h \in \mathcal{H}$, where \mathcal{G} and \mathcal{H} are functional spaces. In the context of magnetic hysteresis, the functional spaces are the applied magnetic field (H) and the magnetic flux density (B). The hysteresis operator $\mathcal{D} : H \rightarrow B$ maps the excitation field functions $h \in H$ to flux density functions $b \in B$. This mapping ensures that $\forall h \in H, \exists b \in B : \mathcal{D}(h) = b$.

In practice, it is challenging to model the hysteresis operator \mathcal{D} analytically, motivating the development of neural surrogates for the operator, which are referred to as neural operators.

The next section describes the methodologies for different neural operators employed in this paper.

III. METHODOLOGY

This section details the approach for modeling magnetic hysteresis through neural operators. As neural operators map functional spaces, the first step in modeling hysteresis involves the selection of input function space, which is the choice for excitation fields. The selection of input space dictates the functions utilized for training and testing the operator. The underlying assumption is that the trained neural operator can effectively generalize to any excitation field within the input functional space. This paper chooses two distinct input spaces corresponding to FORCs and minor loops. Additional details about the generation of functions in the input space are presented in Section IV.

Upon selecting the input space H , excitation fields h are drawn from this space, $h \sim H$. The space H can represent sinusoidal functions, Gaussian random fields, and others, depending on the specific application. The number of samples (N_{sample}) required to obtain a certain approximation accuracy, depends on the complexity of the functional space, the neural operator being employed, and the material under investigation. Since functions must be represented discretely on a computer or from data, the sampling is performed at t_{sample} locations. After generating N_{sample} excitation fields $h \sim H$ at t_{sample} locations, these fields are applied to the material under study to produce the magnetic flux densities. This process yields N_{sample} instances of $b \in B$ corresponding to each $h \sim H$. Consequently, a raw dataset pair (h_i, b_i) is formed, where h_i and b_i each represent a function for each $i, i = 1, \dots, N_{\text{sample}}$.

In cases where the raw dataset pair has to be generated by a Preisach-based model which takes as input B fields and outputs the corresponding H fields, like in this work, the dataset

pair (h_i, b_i) could be generated similarly by first sampling B fields from an appropriate functional space and then generating the corresponding H fields through the Preisach-based model.

Subsequently, the raw dataset is divided randomly into training and testing datasets. This results in two datasets (h_i, b_i) and (h_j, b_j) , with $1 \leq i \leq N_{\text{train}}$, $N_{\text{train}}+1 \leq j \leq N_{\text{train}}+N_{\text{test}}$. Here, N_{train} and N_{test} represent the number of training and test samples with the relation $N_{\text{train}} + N_{\text{test}} = N_{\text{sample}}$. For the numerical experiments considered in this study, the number of training and test samples are kept equal, $N_{\text{train}} = N_{\text{test}}$, to have a fair comparison with recurrent methods. Further details regarding the number of samples are presented in Section IV. The neural operators will be trained with the dataset (h_i, b_i) and tested with (h_j, b_j) . In the rest of the paper, we omit the dependency on time, *i.e.*, h_i and b_i can both denote the functions and those functions sampled at t_{sample} locations. As the fields h_i and h_j are distinct, the operator methods provide a framework to generalize for novel input excitation fields.

The first neural operator employed in this work is the DeepONet. The standard DeepONet architecture [22] is built on fully connected feedforward neural networks as shown in Fig. 1. It comprises two distinct feedforward neural networks, the branch and trunk nets. In this study, the branch net takes functions from the input functional space: the training H fields, h_i . The trunk net takes an array where the output fields are measured, specifically the t_{sample} array. The branch and trunk nets include hidden layers and output neurons, similar to typical feedforward networks.

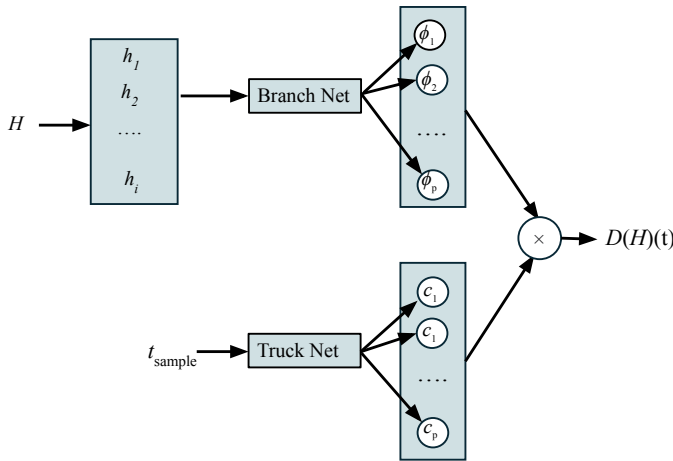


Fig. 1: Deep operator network (DeepONet) architecture. The architecture consists of two separate feedforward neural networks—branch net and trunk net—whose outputs are combined using a dot product to approximate the B fields.

While the number of hidden layers in the branch and trunk nets can vary, the number of outputs is identical. This requirement is necessary because both nets' outputs undergo a dot product operation to approximate the b fields, \hat{b}_i . Mathematically, $b_i \approx \hat{b}_i = \sum_{k=1}^p c_k \phi_k$, where ϕ_k represents the outputs of the branch net and c_k represents the outputs of the trunk net. From a conventional function approximation perspective, ϕ_k can be viewed as basis functions for approximating a function, and c_k as the coefficients of these basis functions, combined

over p terms to approximate the field b_i . The mean-square loss function for DeepONet is,

$$L(\theta) = \frac{1}{N_{\text{train}}} \sum_{i=1}^{N_{\text{train}}} (\hat{b}_i(\theta) - b_i)^2, \quad (1)$$

where the network parameters θ are found through a gradient-based optimization method. Other loss functions minimizing the residual may also be considered using different norms [26].

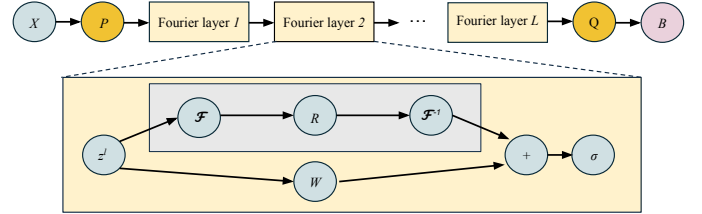


Fig. 2: Neural architecture for Fourier neural operator (FNO) and rate-independent Fourier neural operator (RIFNO). For FNO the input $X := [h_i, t_{\text{sample}}]$, whereas for RIFNO, $X := h_i$. The input is passed through projection tensor (P) and Fourier layers and finally downsampled (Q) to approximate the B field.

The second neural operator employed in this work is FNO, based on convolutional neural network architecture as shown in Fig. 2. FNO does not employ separate networks to process the input fields (h_i) and t_{sample} array; instead, it concatenates them by repeating the t_{sample} array sufficiently to form the input tensor $X := [h_i, t_{\text{sample}}]$ of channel size two. The input X is then passed through a projection tensor, P , to increase the number of channels to N_f , *i.e.*, $z^0 = PX$. The tensor z^0 then undergoes a sequence of Fourier layers, parameterized by learnable tensors W and R . The computations for these Fourier layers can be expressed as,

$$z^{l+1} = \sigma(W^l z^l + \mathcal{F}^{-1}(R^l \mathcal{F}(z^l))), \quad (2)$$

here z^l denotes the latent tensor at l^{th} -layer. First, it undergoes a fast Fourier transform (FFT) \mathcal{F} . Subsequently, first n_m modes are passed through a linear transformation $R \in \mathbb{C}^{\mathcal{F}_{\text{out}} \times \mathcal{F}_{\text{out}}}$ followed by inverse FFT, \mathcal{F}^{-1} , where \mathcal{F}_{out} refers to the dimension of $\mathcal{F}(z^l)$. The obtained tensor is summed with a linearly transformed latent tensor $W^l z^l$. Finally, a nonlinear activation function (σ) is applied to obtain z^{l+1} . These computations are repeated for L number of Fourier blocks. The output of the last Fourier block z^L is then downsampled by two projection tensors Q and \hat{Q} , to obtain the predictions for the fields b_i ,

$$\hat{b}_i = \hat{Q} \sigma(Q z^L). \quad (3)$$

The same loss function (1) as in the case of DeepONet is applied to approximate b_i .

DeepONet and FNO require the magnetic field's measurement grid, the t_{sample} array. However, magnetic hysteresis often exhibits the property of being rate-independent [27]. This paper proposes a minor modification in the FNO architecture to develop a rate-independent Fourier neural operator, namely RIFNO presented in Fig. 2, to incorporate the rate-independent characteristic of magnetic hysteresis. The difference between FNO and RIFNO is the input tensor X , which in the case of

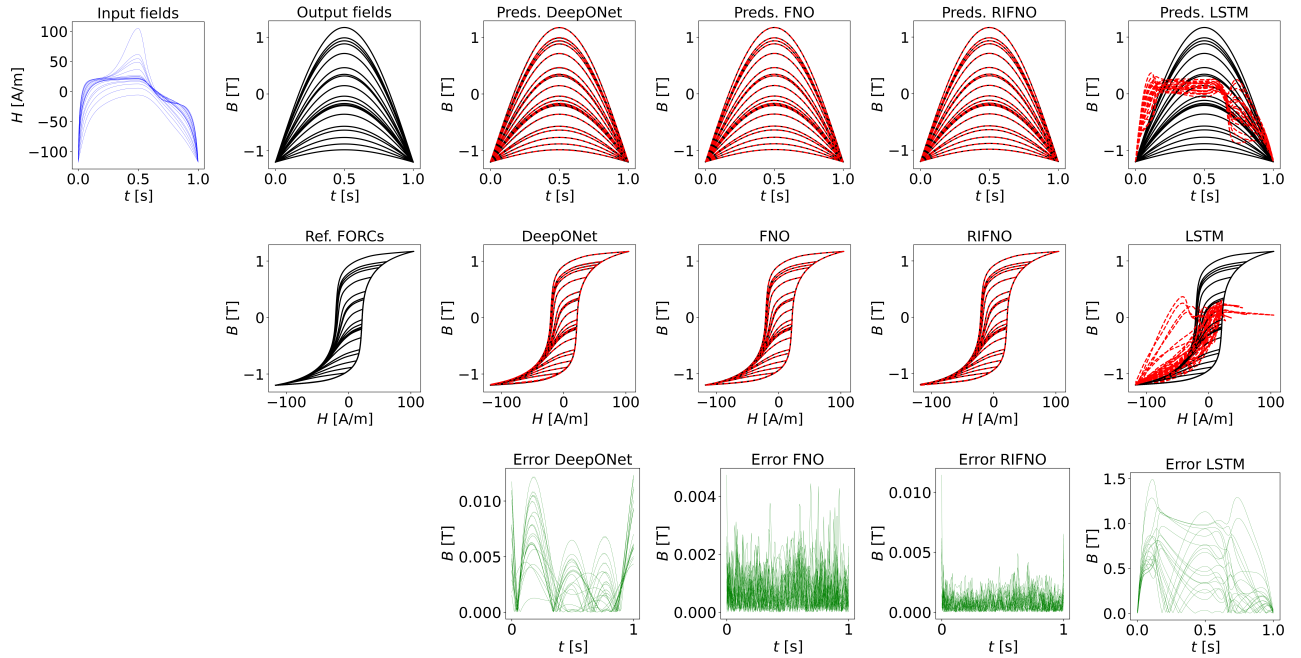


Fig. 3: Performance of neural networks on predicting the first-order reversal curves. **Top row:** (From Left) the input H fields (in blue) for the neural network, the output B fields (in black), followed by the predictions (preds.) of the B fields by DeepONet, FNO, RIFNO, and LSTM, respectively. **Middle row:** (From Left) the reference hysteresis loop (in black) followed by the predicted hysteresis loops (in red) compared with the reference (ref.) loops (in black) for the four methods. **Bottom row:** (From Left) absolute errors in predicting the FORCs for the four methods (in green).

RIFNO is defined as $X = h_i$. Specifically, RIFNO does not concatenate the t_{sample} array with h_i ; hence, the architecture remains invariant to the sampling rate, making it adequate for modeling rate-independent magnetic hysteresis.

IV. NUMERICAL EXPERIMENTS

This section presents the numerical experiments to validate the proposed approach in predicting novel FORCs and minor loops on which training has not been performed. The three neural operator methods are compared with traditional recurrent architectures RNN, LSTM, and GRU to showcase the gain obtained with operators.

The data for the numerical experiments is generated using a Preisach-based method modeling the material NO27-1450H. The measurement data for the Preisach-based method is obtained by a Brockhaus MPG 200 D soft-magnetic material tester, using an Epstein frame calibrated to correspond with the IEC standard. The data are obtained under quasi-DC excitation, indicating that the rate of change of the magnetic flux density is controlled such that any eddy current fields are negligible, and the static hysteresis behavior is obtained. The Epstein sample strips are obtained using spark eroding and cut in the rolling direction.

A. Error metric

Three error metrics are used to quantify the performance of the methods. First is the relative error in \mathbb{L}_2 norm, defined as,

$$\mathcal{R} = \frac{\sqrt{\frac{1}{N_{\text{test}}} \sum_{j=1}^{N_{\text{test}}} (\hat{b}_j - b_j)^2}}{\sqrt{\frac{1}{N_{\text{test}}} \sum_{j=1}^{N_{\text{test}}} b_j^2}}. \quad (4)$$

The second error metric is the mean absolute error (MAE), used to quantify the average absolute difference between the predicted field \hat{b}_j and the actual field b_j , defined as,

$$\text{MAE} = \frac{1}{N_{\text{test}}} \sum_{j=1}^{N_{\text{test}}} |\hat{b}_j - b_j|. \quad (5)$$

The third error metric is the root mean squared error (RMSE) used to quantify the average magnitude of the errors between predicted values \hat{b}_j and actual values b_j , defined as,

$$\text{RMSE} = \sqrt{\frac{1}{N_{\text{test}}} \sum_{j=1}^{N_{\text{test}}} (\hat{b}_j - b_j)^2}. \quad (6)$$

B. First-order reversal curves

The first numerical experiment entails predicting the FORCs. This study employs the Preisach model to generate the dataset for training and testing the neural networks. The model inputs the magnetic flux density (B field) and produces the corresponding magnetic field strength (H field). The b fields are sampled from a functional space B , used as the input for the Preisach model to produce the corresponding H fields. This process generates data pairs (h_i, b_i) , which are used to train the neural networks. Whether one uses experimental data or any other surrogate model characterizing the material, this approach remains invariant to the choice of input sample space and output generated fields.

To generate the dataset for training and testing the neural networks, the functional space of B comprises half sine

curves with amplitudes randomly sampled between 0.1 T and 1.2 T, and defined over the interval $[0, 1]$ with $t_{\text{sample}} = 198$. A total of 2000 sine curves are generated and distributed independently and identically between the training and testing sets, such that $N_{\text{train}} + N_{\text{test}} = 1000 + 1000 = 2000 = N_{\text{sample}}$. Before inputting the data into the neural networks, they are normalized to the range of -1 to 1 using min-max scaling, as described in [11], to facilitate the training process [28].

The first neural operator utilized for modeling FORCs is the DeepONet. The operator uses 1000 random functions as input to the branch net and the t_{sample} array of size 198 as input to the trunk net. The branch and trunk nets are fully connected feedforward neural networks, each comprising eight hidden layers with 200 neurons in each layer and a tanh activation function. The output dimension of both the branch and trunk nets is $p = 100$. The model parameters are initialized using Xavier initialization [29], and the network is trained using the ADAM optimizer with a learning rate of 5×10^{-5} over 10000 epochs.

Further, FNO and RIFNO are employed to predict FORCs. Both architectures share identical structures with variations in input configuration. Specifically, FNO inputs concatenated data consisting of 1000 instances of H fields and a sampling array repeated across 1000 samples, while RIFNO solely utilizes the 1000 instances of H fields as input. Common hyperparameters across both networks include an initial fully connected layer projecting inputs from 2 channels to 8 channels, *i.e.*, $N_f = 8$, followed by four spectral convolutional layers ($L = 4$), each with eight input and eight output channels. Within each block, the first four modes after Fourier transformation are retained ($n_m = 4$). The networks conclude with two fully connected layers transforming dimensions from 8 channels to 128 and finally to a single output channel. ReLU activation function is applied throughout the network. Training parameters encompass a batch size of 100 samples over 10000 epochs, utilizing the ADAM optimizer with a learning rate of 1×10^{-4} .

TABLE I: Errors in predicting first-order reversal curves (\mathcal{R} : relative error in \mathbb{L}_2 norm; MAE: mean absolute error; RMSE: root mean squared error.)

Method	\mathcal{R}	MAE	RMSE
DeepONet	5.84e-3	3.27e-3	4.22e-3
FNO	1.34e-3	7.48e-4	9.74e-4
RIFNO	1.63e-3	8.79e-4	1.17e-3
RNN	1.19e+0	6.99e-1	8.61e-1
LSTM	8.08e-1	4.76e-1	5.83e-1
GRU	9.27e-1	5.18e-1	6.70e-1

The neural operators are subsequently benchmarked against traditional recurrent architectures, specifically RNN, LSTM, and GRU. Following the data processing similar to [11], [13], the input and output dimensions are set to 1000 for each cell. The sequence length is fixed at 198, corresponding to the size of the sampling array, t_{sample} . Each recurrent cell consists of 128 neurons with a single hidden layer. Training spans 10000 epochs using the ADAM optimizer with a learning rate 1×10^{-4} .

Fig. 3 illustrates the input and output fields for training

neural networks and corresponding results for the neural operators and sequential model in predicting magnetic hysteresis. The first row shows the input fields (blue curves) and output fields (black curves), along with predictions from four models: DeepONet, FNO, RIFNO, and LSTM, with FNO demonstrating the best approximation. The second row compares the FORC predictions for each model, where red curves indicate predictions and black curves show the ground truth. The third row presents absolute error plots, showcasing that LSTM performs poorly with widespread errors. The error for DeepONet propagates sinusoidally, FNO has a maximum error of 0.004, and the error in RIFNO predictions are prominent near the ends. Overall, neural operators perform better in approximating magnetic hysteresis than the recurrent neural methods.

Additionally, Table I compares the prediction errors for FORCs across six models: DeepONet, FNO, RIFNO, RNN, LSTM, and GRU, using three metrics: relative error (\mathcal{R}), MAE, and RMSE. FNO exhibits the lowest errors ($\mathcal{R} = 1.34\text{e-}3$, MAE = 7.48e-4, RMSE = 9.74e-4), demonstrating superior accuracy. RIFNO also performs well with slightly higher errors ($\mathcal{R} = 1.63\text{e-}3$, MAE = 8.79e-4, RMSE = 1.17e-3). DeepONet also captures the hysteresis well but with an order of magnitude less accuracy than FNO. In contrast, RNN, LSTM, and GRU show higher errors and cannot capture the hysteresis and predict for novel input H fields. Table I underscores the effectiveness of FNO in accurately predicting first-order reversal curves, followed by RIFNO and DeepONet, while traditional recurrent models underperform.

C. Rate-independency

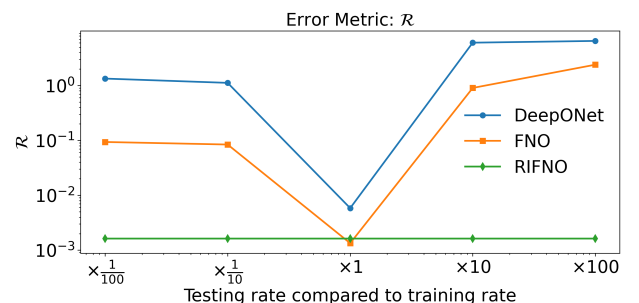


Fig. 4: Variation of relative error with respect to different testing rates for neural operators.

This experiment evaluates the predictive capability of the trained FORC models under varying sampling rates during testing, differing from the training rate. Specifically, the original sampling array, $[0, 1]$, consisting of equispaced 198 points, is now tested using arrays $[0, 0.01]$, $[0, 0.1]$, $[0, 10]$, and $[0, 100]$ each at equispaced 198 points, corresponding to sampling rates of 1/100, 1/10, 10, and 100 times the rate used in training. This investigation aims to assess the model's ability to generalize across different sampling rates and determine if it maintains the rate-independent property of magnetic hysteresis.

Fig. 4 shows the error metric \mathcal{R} for DeepONet, FNO, and RIFNO across different testing rates compared to the training

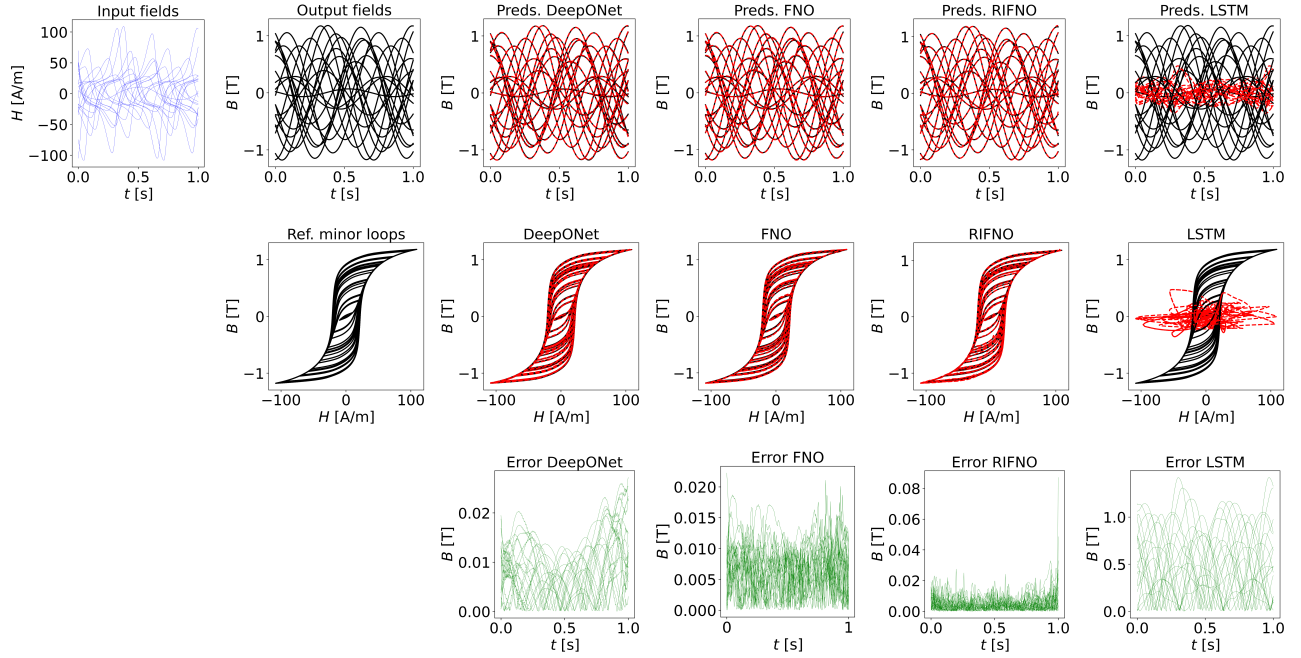


Fig. 5: Performance of neural networks on predicting the minor loops. **Top row:** (From Left) the input H fields (in blue) for the neural network, the output B fields (in black), followed by the predictions (preds.) of the B fields by DeepONet, FNO, RIFNO, and LSTM, respectively. **Middle row:** (From Left) the reference hysteresis loop (in black) followed by the predicted hysteresis loops (in red) compared with the reference (ref.) loops (in black) for the four methods. **Bottom row:** (From Left) absolute errors in predicting the minor loops for the four methods (in green).

TABLE II: Errors for testing on different rates

Rate	Metric	DeepONet	FNO	RIFNO
$\times \frac{1}{100}$	\mathcal{R}	1.34e+0	9.37e-2	1.63e-3
	MAE	7.72e-1	5.25e-2	8.79e-4
	RMSE	9.71e-1	6.77e-2	1.17e-3
$\times \frac{1}{10}$	\mathcal{R}	1.12e+0	8.42e-2	1.63e-3
	MAE	6.37e-1	4.71e-2	8.79e-4
	RMSE	8.14e-1	6.08e-2	1.17e-3
$\times 10$	\mathcal{R}	6.05e+0	9.05e-1	1.63e-3
	MAE	3.71e+0	4.89e-1	8.79e-4
	RMSE	4.37e+0	6.54e-1	1.17e-3
$\times 100$	\mathcal{R}	6.51e+0	2.40e+0	1.63e-3
	MAE	4.20e+0	1.35e+0	8.79e-4
	RMSE	4.70e+0	1.73e+0	1.17e-3

rate. The line graph demonstrates the variation of error for each model concerning the testing rate from $\frac{1}{100}$ to 100 times the training rate. RIFNO exhibits the lowest and most consistent errors across all testing rates, indicating its superior generalization capability. FNO has higher errors compared to RIFNO. DeepONet shows the highest errors, especially at extreme testing rates, highlighting its comparatively lower robustness in varying conditions. Fig. 4 underscores the efficacy of RIFNO in maintaining low prediction errors across various testing scenarios, making it the most accurate operator among the three where different testing rates are considered.

Table II presents the errors in predicting the first-order reversal curve for different testing rates compared to the training rate using the DeepONet, FNO, and RIFNO models. The testing rates vary as $\frac{1}{100}$, $\frac{1}{10}$, 10, and 100 times the training rate, and the table includes three error metrics. For the $\frac{1}{100}$ rate, RIFNO demonstrates the lowest errors with $\mathcal{R} = 1.63e-3$,

MAE = $8.79e-4$, and RMSE = $1.17e-3$, outperforming DeepONet and FNO. This trend continues across all testing rates, with RIFNO consistently showing minimal errors, indicating its robustness and superior accuracy. In contrast, DeepONet exhibits the highest errors, especially at extreme testing rates. FNO performs better than DeepONet but still shows increasing errors as the testing rate deviates from the training rate.

D. Minor loops

TABLE III: Errors in predicting minor loops

Method	\mathcal{R}	MAE	RMSE
DeepONet	1.80e-2	8.40e-3	1.00e-2
FNO	1.44e-2	7.08e-3	8.07e-3
RIFNO	1.26e-2	5.07e-3	7.03e-3
RNN	1.15e+0	5.25e-1	6.43e-1
LSTM	1.02e+0	4.74e-1	5.71e-1
GRU	1.06e+0	4.91e-1	5.95e-1

In the final numerical experiment, minor loops are predicted. The dataset for training and testing neural networks consists of functions generated using the cosine kernel of Gaussian processes. The input domain is $[0, 3\pi]$, with 198 evenly spaced points. These points are used with a cosine kernel to define covariance functions from which function samples are drawn. Each sample adheres to a maximum threshold of 1.2 T. A total of 2000 sine curves are generated and evenly split between training and testing sets, ensuring $N_{\text{train}} + N_{\text{test}} = 2000$. Consistent network hyperparameters are applied across all methods to maintain alignment with FORC prediction cases.

TABLE IV: Comparison of recurrent and operator architectures based on various attributes

Attributes	Methods					
	RNN	LSTM	GRU	DON	FNO	RIFNO
Predictions on trained excitation fields	✓	✓	✓	✓	✓	✓
Preserves magnetization-demagnetization history	✓	✓	✓	✓	✓	✓
Maps functions to functions	×	×	×	✓	✓	✓
Predictions on novel excitation fields	×	×	×	✓	✓	✓
Rate-independent	✓	✓	✓	×	×	✓

Fig. 5 illustrates the performance of various neural operator methods in predicting the minor loops. The first row shows input fields (blue curves) and output fields (black curves), along with predictions from DeepONet, FNO, RIFNO, and LSTM, with RIFNO providing the most accurate approximations. The second row presents the minor loop curves, comparing predicted (red curves) and actual (black curves) output fields, demonstrating that FNO closely matches the ground truth. The third row displays absolute error plots, revealing that LSTM performs poorly with higher errors. The errors for DeepONet follow a specific pattern, while the errors for FNO predictions are minimal, with a maximum of approximately 0.02, and RIFNO errors are prominent near the ends.

Table III compares prediction errors for minor loops across six models: DeepONet, FNO, RIFNO, RNN, LSTM, and GRU, using relative error (\mathcal{R}), MAE, and RMSE. RIFNO achieves the lowest errors ($\mathcal{R} = 1.26e-2$, MAE = 5.07e-3, RMSE = 7.03e-3), indicating superior accuracy. FNO and DeepONet follow with slightly higher errors than RIFNO. Conversely, traditional recurrent models like RNN, LSTM, and GRU show significantly higher errors, with LSTM and GRU performing the worst. Table III underscores the leading performance of RIFNO, followed by FNO and DeepONet, while traditional recurrent models lag in modeling novel minor loops not used for training the neural network model.

V. DISCUSSION

This section discusses key implications following the successful application of neural operators in modeling hysteresis. The presented numerical experiments on FORCs and minor loops demonstrate that neural operators accurately predict the magnetic field response $b \sim B$ corresponding to $h \sim H$, whether h is part of the training data or not. In contrast, recurrent architectures only reliably predict responses for h values within the training set, highlighting a limitation for applications requiring predictions for novel magnetic fields. Moreover, once trained, neural operators enable real-time inference, enhancing their utility in applications such as control.

A comparative analysis between recurrent and operator-based methods is presented in Table IV, focusing on essential attributes for modeling magnetic hysteresis. Table IV illustrates that operator learning methods excel in mapping arbitrary H fields to B fields while preserving the history of magnetization and demagnetization. The recurrent networks are rate-independent owing to their architecture, which does not explicitly include the rate at which the data is collected. RIFNO provides an advantage over recurrent and other operator networks by offering function-to-function mapping and rate independence properties.

Fundamentally, the results bridge the gap between hysteresis modeling and SciML. The evolution of SciML has led to the development of a plethora of operator learning methods to accelerate the modeling and simulation of physical systems, including but not limited to [30]–[32]. These operator learning methods could be employed to model hysteresis and advance modeling of magnetic materials. The bridge between hysteresis modeling and SciML also presents an avenue to benchmark the results and datasets as advocated in [33].

Future research directions include employing and developing different operator training methods. Techniques like transfer learning [34], leveraging pre-trained network parameters [35], and meta-learning approaches [36] can be utilized to accelerate model convergence. Additionally, the results presented herein for scalar hysteresis could be expanded upon to model vector hysteresis, leveraging the property that deep learning often circumvents the curse of dimensionality and generalizes well to higher dimensions.

VI. CONCLUSIONS

This paper introduced a novel approach to model magnetic hysteresis through deep learning. The research highlights the benefits of employing neural operators for hysteresis modeling, yielding generalizable models essential for scenarios where prior training on varying magnetic fields is impractical. By employing prominent operator networks, namely deep operator network and Fourier neural operator, the research demonstrated the prediction of novel first-order reversal curves and minor loops outperforming the traditional recurrent architectures and leading to the development of generalizable neural hysteresis models. Furthermore, this contribution introduced a rate-independent Fourier neural operator, which enhanced the neural operator framework by incorporating the rate-independent hysteresis characteristics prevalent in magnetic materials. Concretely, this paper advances neural hysteresis modeling by developing accurate and generalizable models capable of real-time inference of material responses. The codes and dataset related to the work will be made available upon publication.

REFERENCES

- [1] G. Bertotti and I. D. Mayergoyz, *The science of hysteresis: 3-volume set*. Elsevier, 2005.
- [2] I. Mayergoyz, “Mathematical models of hysteresis,” *IEEE Transactions on Magnetics*, vol. 22, no. 5, pp. 603–608, 1986.
- [3] D. C. Jiles and D. L. Atherton, “Theory of ferromagnetic hysteresis,” *Journal of Magnetism and Magnetic Materials*, vol. 61, no. 1-2, pp. 48–60, 1986.
- [4] F. Preisach, “Über die magnetische nachwirkung,” *Zeitschrift für Physik*, vol. 94, no. 5, pp. 277–302, 1935.

- [5] G. Mörée and M. Leijon, "Review of hysteresis models for magnetic materials," *Energies*, vol. 16, no. 9, p. 3908, 2023.
- [6] N. Vuokila, C. Cuning, J. Zhang, N. Akel, A. Khan, and D. A. Lowther, "The application of neural networks to the modeling of magnetic hysteresis," *IEEE Transactions on Magnetics*, 2023.
- [7] A. Adly and S. Abd-El-Hafiz, "Field computation in media exhibiting hysteresis using hopfield neural networks," *IEEE Transactions on Magnetics*, vol. 58, no. 2, pp. 1–5, 2021.
- [8] Z. He, J.-S. Kim, and C.-S. Koh, "An improved model for anomalous loss utilizing loss separation and comparison with ann model in electrical steel sheet," *IEEE Transactions on Magnetics*, vol. 58, no. 9, pp. 1–5, 2022.
- [9] D. Serrano, H. Li, T. Guillod, S. Wang, M. Luo, C. R. Sullivan, and M. Chen, "Neural network as datasheet: modeling B-H loops of power magnetics with sequence-to-sequence LSTM encoder-decoder architecture," in *2022 IEEE 23rd Workshop on Control and Modeling for Power Electronics (COMPEL)*. IEEE, 2022, pp. 1–8.
- [10] S. Cao, B. Wang, J. Zheng, W. Huang, L. Weng, and W. Yan, "Hysteresis compensation for giant magnetostrictive actuators using dynamic recurrent neural network," *IEEE Transactions on Magnetics*, vol. 42, no. 4, pp. 1143–1146, 2006.
- [11] A. Chandra, T. Kapoor, B. Daniels, M. Curti, K. Tiels, D. M. Tartakovsky, and E. A. Lomonova, "Neural oscillators for magnetic hysteresis modeling," *arXiv preprint arXiv:2308.12002*, 2023.
- [12] H. Zhang, Q. Yang, C. Zhang, Y. Li, and Y. Chen, "Magnetic properties simulation of electrical steel sheet based on recurrent neural network," *IEEE Transactions on Magnetics*, 2023.
- [13] H. Li, D. Serrano, T. Guillod, S. Wang, E. Dogariu, A. Nadler, M. Luo, V. Bansal, N. K. Jha, Y. Chen *et al.*, "How magnet: machine learning framework for modeling power magnetic material characteristics," *IEEE Transactions on Power Electronics*, 2023.
- [14] T. Kapoor, A. Chandra, D. M. Tartakovsky, H. Wang, A. Nunez, and R. Dollevoet, "Neural oscillators for generalization of physics-informed machine learning," in *Proceedings of the AAAI Conference on Artificial Intelligence*, vol. 38, no. 12, 2024, pp. 13 059–13 067.
- [15] Y. LeCun, Y. Bengio, and G. Hinton, "Deep learning," *Nature*, vol. 521, no. 7553, pp. 436–444, 2015.
- [16] S. Hochreiter and J. Schmidhuber, "Long short-term memory," *Neural Computation*, vol. 9, no. 8, pp. 1735–1780, 1997.
- [17] K. Cho, B. Van Merriënboer, C. Gulcehre, D. Bahdanau, F. Bougares, H. Schwenk, and Y. Bengio, "Learning phrase representations using rnn encoder-decoder for statistical machine translation," *arXiv preprint arXiv:1406.1078*, 2014.
- [18] T. Chen and H. Chen, "Universal approximation to nonlinear operators by neural networks with arbitrary activation functions and its application to dynamical systems," *IEEE Transactions on Neural Networks*, vol. 6, no. 4, pp. 911–917, 1995.
- [19] K. Azizzadenesheli, N. Kovachki, Z. Li, M. Liu-Schiaffini, J. Kossaifi, and A. Anandkumar, "Neural operators for accelerating scientific simulations and design," *Nature Reviews Physics*, pp. 1–9, 2024.
- [20] N. Kovachki, Z. Li, B. Liu, K. Azizzadenesheli, K. Bhattacharya, A. Stuart, and A. Anandkumar, "Neural operator: Learning maps between function spaces with applications to PDEs," *Journal of Machine Learning Research*, vol. 24, no. 89, pp. 1–97, 2023.
- [21] L. Lu, X. Meng, S. Cai, Z. Mao, S. Goswami, Z. Zhang, and G. E. Karniadakis, "A comprehensive and fair comparison of two neural operators (with practical extensions) based on fair data," *Computer Methods in Applied Mechanics and Engineering*, vol. 393, p. 114778, 2022.
- [22] L. Lu, P. Jin, G. Pang, Z. Zhang, and G. E. Karniadakis, "Learning nonlinear operators via DeepONet based on the universal approximation theorem of operators," *Nature Machine Intelligence*, vol. 3, no. 3, pp. 218–229, 2021.
- [23] Z. Li, N. B. Kovachki, K. Azizzadenesheli, K. Bhattacharya, A. Stuart, A. Anandkumar *et al.*, "Fourier neural operator for parametric partial differential equations," in *International Conference on Learning Representations*, 2020.
- [24] K. Hornik, M. Stinchcombe, and H. White, "Multilayer feedforward networks are universal approximators," *Neural Networks*, vol. 2, no. 5, pp. 359–366, 1989.
- [25] H. T. Siegelmann and E. D. Sontag, "On the computational power of neural nets," in *Proceedings of the Fifth Annual Workshop on Computational Learning Theory*, 1992, pp. 440–449.
- [26] T. Kapoor, H. Wang, A. Núñez, and R. Dollevoet, "Predicting traction return current in electric railway systems through physics-informed neural networks," in *2022 IEEE Symposium Series on Computational Intelligence (SSCI)*. IEEE, 2022, pp. 1460–1468.
- [27] X. Xiao, A. C. Thul, L. E. Müller, and K. Hameyer, "Basic properties of ferromagnetic vector hysteresis play models and their validation by finite element method," *COMPEL-The International Journal for Computation and Mathematics in Electrical and Electronic Engineering*, 2024.
- [28] T. Kapoor, H. Wang, A. Núñez, and R. Dollevoet, "Physics-informed neural networks for solving forward and inverse problems in complex beam systems," *IEEE Transactions on Neural Networks and Learning Systems*, 2023.
- [29] X. Glorot and Y. Bengio, "Understanding the difficulty of training deep feedforward neural networks," in *Proceedings of the Thirteenth International Conference on Artificial Intelligence and Statistics*. JMLR Workshop and Conference Proceedings, 2010, pp. 249–256.
- [30] L. Yang, S. Liu, T. Meng, and S. J. Osher, "In-context operator learning with data prompts for differential equation problems," *Proceedings of the National Academy of Sciences*, vol. 120, no. 39, p. e2310142120, 2023.
- [31] B. Raonic, R. Molinaro, T. De Ryck, T. Rohner, F. Bartolucci, R. Alai-fari, S. Mishra, and E. de Bézenac, "Convolutional neural operators for robust and accurate learning of PDEs," *Advances in Neural Information Processing Systems*, vol. 36, 2024.
- [32] V. Fanaskov and I. V. Oseledets, "Spectral neural operators," in *Doklady Mathematics*, vol. 108, no. Suppl 2. Springer, 2023, pp. S226–S232.
- [33] H. Li, D. Serrano, S. Wang, and M. Chen, "Magnet-AI: Neural network as datasheet for magnetics modeling and material recommendation," *IEEE Transactions on Power Electronics*, 2023.
- [34] F. Zhuang, Z. Qi, K. Duan, D. Xi, Y. Zhu, H. Zhu, H. Xiong, and Q. He, "A comprehensive survey on transfer learning," *Proceedings of the IEEE*, vol. 109, no. 1, pp. 43–76, 2020.
- [35] T. Kapoor, H. Wang, A. Núñez, and R. Dollevoet, "Transfer learning for improved generalizability in causal physics-informed neural networks for beam simulations," *Engineering Applications of Artificial Intelligence*, vol. 133, p. 108085, 2024.
- [36] T. Hospedales, A. Antoniou, P. Micaelli, and A. Storkey, "Meta-learning in neural networks: A survey," *IEEE Transactions on Pattern Analysis and Machine Intelligence*, vol. 44, no. 9, pp. 5149–5169, 2021.